Journal of Advanced Research xxx (xxxx) xxx

Contents lists available at ScienceDirect

Journal of Advanced Research

journal homepage: www.elsevier.com/locate/jare

Original Manuscript

New molecular mechanisms to explain the neuroprotective effects of insulin-like growth factor II in a cellular model of Parkinson's disease

Silvana-Yanina Romero-Zerbo [a,1], Nadia Valverde [b,1], Silvia Claros [a,1], Pablo Zamorano-Gonzalez [a], Federica Boraldi [c], Francesco-Demetrio Lofaro [c], Estrella Lara [a], Jose Pavia [b,*], Maria Garcia-Fernandez [a,*], Belen Gago [a,1], Elisa Martin-Montañez [b,1]

[a] Departamento de Fisiología Humana, Facultad de Medicina, Instituto de Investigación Biomédica de Málaga (IBIMA), Universidad de Málaga (UMA), Malaga 29010, Spain
[b] Departamento de Farmacología y Pediatría, Facultad de Medicina, Instituto de Investigación Biomédica de Málaga (IBIMA), Universidad de Málaga (UMA), Malaga 29010, Spain
[c] Dipartimento di Scienze Della Vita. Patologia Generale, Universita di Modena e Reggio Emilia 4112, Italy

HIGHLIGHTS

- IGF-II improves mitochondrial dynamics through Mitofilin.
- IGF-II rebalances the cell cycle, reducing apoptosis and cell death.
- IGF-II stimulates cellular mechanisms to protect DNA integrity.
- IGF-II regulates transcription factors, such as Checkpoint kinase 1.
- The neuroprotective effect is due to its continuous presence in the medium.

GRAPHICAL ABSTRACT

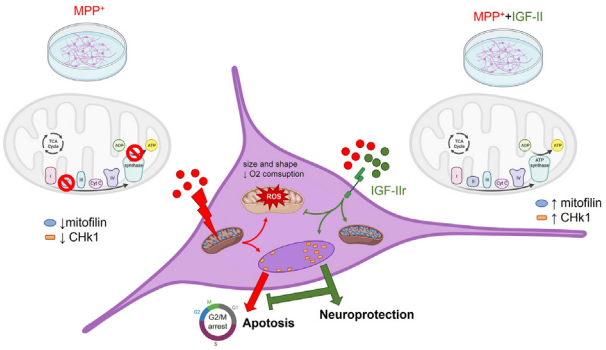

ARTICLE INFO

Article history:
Received 6 September 2023
Revised 31 January 2024
Accepted 31 January 2024
Available online xxxx

Keywords:
Parkinsońs disease
IGF-II
Neuroprotection
Mitochondria
Cell cycle

ABSTRACT

Introduction: One of the hallmarks of Parkinsońs Disease (PD) is oxidative distress, leading to mitochondrial dysfunction and neurodegeneration. Insulin-like growth factor II (IGF-II) has been proven to have antioxidant and neuroprotective effects in some neurodegenerative diseases, including PD. Consequently, there is growing interest in understanding the different mechanisms involved in the neuroprotective effect of this hormone.
Objectives: To clarify the mechanism of action of IGF-II involved in the protective effect of this hormone.
Methods: The present study was carried out on a cellular model PD based on the incubation of dopaminergic cells (SN4741) in a culture with the toxic 1-methyl-4-phenylpyridinium (MPP^+), in the presence of IGF-II. This model undertakes proteomic analyses in order to understand which molecular cell pathways might be involved in the neuroprotective effect of IGF-II. The most important proteins found in the proteomic study were tested by Western blot, colorimetric enzymatic activity assay and immunocytochemistry. Along with the proteomic study, mitochondrial morphology and function were also studied by transmission electron microscopy and oxygen consumption rate. The cell cycle was also analysed using 7AAd/BrdU staining, and flow cytometry.
Results: The results obtained indicate that MPP^+, MPP^++IGF-II treatment and IGF-II, when compared to control, modified the expression of 197, 246 proteins and 207 respectively. Some of these proteins were

* Corresponding authors.
E-mail addresses: pavia@uma.es (J. Pavia), igf@uma.es (M. Garcia-Fernandez).
[1] Equally contributed.

https://doi.org/10.1016/j.jare.2024.01.036

Please cite this article as: S.-Y. Romero-Zerbo, N. Valverde, S. Claros et al., New molecular mechanisms to explain the neuroprotective effects of insulin-like growth factor II in a cellular model of Parkinson's disease, Journal of Advanced Research, https://doi.org/10.1016/j.jare.2024.01.036

found to be involved in mitochondrial structure and function, and cell cycle regulation. Including IGF-II in the incubation medium prevents the cell damage induced by MPP^+, recovering mitochondrial function and cell cycle dysregulation, and thereby decreasing apoptosis.

Conclusion: IGF-II improves mitochondrial dynamics by promoting the association of Mitofilin with mitochondria, regaining function and redox homeostasis. It also rebalances the cell cycle, reducing the amount of apoptosis and cell death by the regulation of transcription factors, such as Checkpoint kinase 1.

Introduction

Parkinson's disease (PD), which is the most common body movement disorder, is a neurodegenerative disease affecting 3 % of the aged population [1]. This disease is characterised by the progressive loss of nigral dopaminergic neurons (DA), leading to core motor symptoms such as bradykinesia, resting tremor or rigidity. This DA degeneration is mediated, among others, by oxidative stress, protein misfolding and aggregation, mitochondrial dysfunction and neuroinflammation [2]. A clearer understanding of the vulnerability mechanisms of DA neurons and/or their connections would be important to the development of novel laboratory strategies and therapies. In this study, we have used a previously established cellular model of PD based on the administration of the neurotoxin MPP^+ to SN 4741 cells in culture [3,4].

The common role of oxidative stress and mitochondrial dysfunction in apoptosis and cell death appears clear in the pathogenesis of the neurodegenerative disorders [5,6]. However, cell cycle entry could also play a key part in neurodegeneration, as suggested by the numerous hallmarks of cell cycle activation described in a variety of neurodegenerative disorders, including PD [7,8]. Furthermore, oxidative-DNA damage and mitochondrial dysfunction are involved in neuronal cell cycle activation in PD [9]. Thus, after oxidative injury, DNA damage response is activated, inducing DNA replication and cell cycle entry, and thus, to DNA repair. However, dysregulation during this process in pathological conditions can result in an aberrant cell cycle and apoptosis [8]. Mitochondrial ATP production is also impaired by DNA damage and other damaging stimuli, leading to the activation of AMP-activated protein kinase, which, in turn, triggers defects at G_1/S transition and G_2/M arrest [7].

In recent years, the role of the pleiotropic hormone Insulin-like Growth Factor II (IGF-II) in modulating processes, such as learning and memory, neurogenesis, synaptic plasticity and modulation of neurotransmitter release, has been increasingly understood [10,11]. Also, its reported role as a key neuroprotective factor in pathological conditions has gradually attracted interest to this molecule specially as a therapeutic approach in neurodegenerative diseases [12–14].

At present, IGF-II has shown neuroprotective and antioxidant effects in aging situations [15], stress conditions mediated by glucocorticoids [16,17], autism [18], schizophrenia [19,20], Alzheimer's disease [21] and PD [3]. This hormone, broadly distributed in the central nervous system, mediates its functions by interacting with its specific receptor, IGF-II/Mannose 6-Phosphate receptor (IGF-IIr), as well as with the insulin-like growth factor I receptors and all insulin receptors. The expression of these receptors is elevated in adult brain areas, including the substantia nigra [22].

Recently, our group has shown the IGF-II neuroprotective effect against oxidative damage to work mainly, but not exclusively, through its interaction with the specific IGF-IIr, in neuronal cell cultures [3,16,17,23]. It was demostrated that inclusion of IGF-II in the treatment of cells leads to the recovery of oxidative balance, mitochondrial morphology and function, and restoration of cellular bioenergetics; although a greater understanding of these IGF-II neuroprotective mechanisms and their connections is still needed. A complete evaluation of these mechanisms, together with a structural and functional analysis of proteins involved in the mechanisms described above, could provide a comprehensive map of the proteins interactions associated with the neuroprotective effect of this hormone in order to improve the knowledgement of IGF-II action mechanisms and evaluate its potential use in PD treatment.

This study looks at the molecular mechanisms leading to the neuroprotective effect of IGF-II, based on the previous results obtained in an mouse model of Parkinson's disease after chronic administration of MPTP [3] for five weeks.

Material and methods

Cell culture

The cell line SN4741 (RRID:CVCL S466) is an embryonic cell line expressing dopaminergic neurons from mouse substantia nigra [4] (kindly provided by Prof. Ernest Arenas, Karolinska Institute, Stockholm). These neurons were maintained at 37 °C and a 5 % CO_2 atmosphere in D-MEM high-glucose (Thermo Fisher Scientific, Waltham, MA, USA) supplemented with 10 % FBS and 1 % penicillin/streptomycin (Thermo Fisher Scientific, Waltham, MA, USA). For the experiments, cells were seeded and incubated in plates for 24 h (up to 70–80 % confluence).

Cellular treatment

The treatments were performed with toxic MPP^+ (400 μM) (Cas n° 36913–39-0, SIGMA), IGF-II (25 ng/mL) (Lilly Laboratories [Madrid, Spain]), and the inhibitor of tyrosine kinase effect of the IGF-I receptor and Insulin receptor, BMS-536924 (BMS) (1 μM) (Cas n° 468740-43-4, TOCRIS) and 5 μg/mL anti-IGF-IIR (AB) (R&D Systems, USA Catalog # 2447-GR). BMS was dissolved in DMSO and modified Locke solution (the concentration of DMSO was always less than 0.001 %). The remaining compounds were dissolved in modified Locke's solution (NaCl 137 mM, $CaCl_2$ 5 mM, KCl 10 mM, glucose 25 mM, Hepes 10 mM, pH 7.4)) with L-glutamine (2 mM). The concentrations of IGF-II and MPP^+ were chosen from previous viability experiments with different concentrations of the drugs [17,23]. The concentrations of BMS and AB were chosen based on the provider's recommendation after checking that this concentration did not trigger any apoptotic process in our cells (data not shown).

The exposure to drugs consisted in a two phases paradigm. Firstly, cells were washed with PBS and incubated with either MPP^+, MPP^++IGF-II, MPP^++IGF-II + BMS (or AB) or IGF-II in Lockés solution for two hours [16]. Secondly, after this time, MPP^+ was removed from the medium and cells were maintained in Lockés solution (MPP^+ treated cells), or in the presence of IGF-II (MPP^++-IGF-II and control + IGF-II cells (CO + IGF-II)), or IGF-II + BMS or antibody (MPP^++IGF-II + BMS or antibody) diluted in Lockés solution for two additional hours. Untreated control cells (CO) were maintained in Lockés solution with the same media changes as

the other groups. All the experiments were carried out after the second two-hour period.

Transmission electron microscopy (TEM)

Cells were cultured in plates, and after the treatments with MPP^+ or IGF-II or MPP^++IGF-II, they were removed and fixed with 2.5 % glutaraldehyde in 0.1 M cacodylate buffer at pH 7.4 for 4 h and then in 1 % osmium in cacodylate buffer for 1 h at 4 °C. The remaining protocol was performed as previously described [24]. Ultrathin sections (60–70 nm) were obtained, mounted on 150-mesh copper grids and stained with UranyLess (Electron Microscopy Sciences) and lead citrate. The samples were observed with a FEI NOVA NanoSEM 450 microscopy. To understand effects on mitochondrial size and shape, mitochondria were analysed using Image J software (National Institute of Health; https://rsbweb.nih.gov/ij/) considering six mitochondrial indexes [25]: surface area (mitochondrial size); external perimeter; aspect ratio ((major axis)/(minor axis)) of each mitochondrion; circularity (4π*(area)/(perimeter^2)); roundness (4*(area)/π*(major axis^2)); and form factor ((perimeter^2)/(4π*surface area)). The analyses were performed on 100 mitochondria for each experimental group using Image J software.

Seahorse study

Mitochondrial oxygen consumption rate

The mitochondrial oxygen consumption rate (OCR) was set in real-time using the Seahorse Bioscience XF24 analyser (Agilent Technologies, Santa Clara, CA, USA). For this, cells were seeded in 24-well plates (20,000 cells/well) and incubated with Agilent Seahorse XF Base Medium (without phenol red and bicarbonate) containing pyruvate (1 mM) and glucose (25 mM). The OCR measurement was performed using the instruction provided with the commercial Seahorse XF cell Mito Stress test kit (Agilent Technologies, USA) [26,27]. OCRs were normalised according to protein concentration measured by Bradford assay (Thermo Scientific™ Pierce™ Bradford Protein Assay Kits, USA) [28].

Proteomic analysis

Protein extraction and preparation

Protein extraction was performed on frozen cells after their lysis in modified RIPA buffer (1 % NP-40; 150 mm NaCl; 1 % SDS and protease inhibitor cocktail) and homogenization by a G19 needle and incubation 30 min in ice. Lysates were cleared by centrifugation and samples were precipitated in pure acetone for one hour at −80 °C. Each replicate was centrifuged for 30 min at 14,000 g and protein pellets were washed in pure acetone and centrifuged for 5 min at 14,000 g at 4 °C. Lastly, pellets were resuspended in 50 mM NH_4HCO_3 and protein concentration was determined by Bradford assay. Extraction was performed on two samples for each condition (control, MPP^+, IGF-II-MPP^+, IGF-II) each sample containing 10^6 cells from three different wells.

For each replicate, solution digestion was performed using 50 µg of proteins. Proteins were reduced and alkylated and subsequently digested with trypsin solution (Promega, Madison, WI, USA), buffered in 50 mM NH_4HCO_3, overnight at 37 °C using an enzyme-to-protein ratio of 1:50 (w/w) [24]. All the reagents were purchased from Sigma-Aldrich (Germany) unless otherwise stated.

Liquid chromatography and mass spectrometry (LC-MS/MS)

LC-MS/MS was performed on an UHPLC ultimate 3000 system coupled to a Q Exactive Hybrid Quadrupole-Orbitrap Mass Spectrometer (Thermo Fisher Scientific, Waltham, MA, USA) [24]. Chromatographic separation of peptides took place in a reverse-phase C18 column (50 mm × 2.1 µm ID, 1.8 µm, Zorbax) and elution was performed using a binary system of solvent. Mobile phase A consisted of 0.1 % formic acid in ultrapure water. Mobile phase B was 0.1 % formic acid in acetonitrile. For separation, a linear binary gradient was applied: 2–3 % B for 5 min, to 28 % B for the next 59 min, and then 90 % B for 7 min. The column was maintained at 30 °C and the flow rate used was 0.3 mL/min. The precursor ion detection was carried out in an m/z-range from 200 to 2000, and the acquisition range for fragment ions was m/z from 200 to 2000. Data acquisition was controlled by Xcalibur 2.0.7 Software (Thermo Fisher Scientific, USA) [24].

Data analysis

The MS/MS ion search was performed by the MASCOT server (v.2.7.0; Matrix Science), converting raw ms/ms using default settings of msConvert ProteoWizard (v.3.0.19239) to MGF file. Parameters set for identification included: i) cRAP and Uniprot (2018_05) restricted to Mus musculus (Taxon ID: 10,090) were selected for database search; ii) trypsin as the enzyme with 1 as the maximum missed cleavage; iii) mass error tolerances for precursor and fragment ions set to 10 ppm and 0.02 Da, respectively; iv) peptide charge (2+, 3+, 4+); v) protein mass no restriction; vi) carbamidomethyl cysteine was set as fixed modification, while deamidation of asparagine and glutamine and oxidation of methionine were considered as dynamic modification. Label-free quantification was performed using emPAI reported by MASCOT. Only peptides confident identified, with a false discovery rate ≤1 % and proteins with at least two unique peptides were exported. Relative abundance (emPAI) was calculated in each sample by dividing the emPAI value by the sum of all emPAI values. Proteins were considered up- or down-regulated when the $\log_2$ fold change is more than 1 or less than −1, respectively.

Protein-protein interaction network and functional enrichment analysis of the network obtained were carried out using STRING v.11.0 [29]. The Venn diagram was built using Venny (v.2.1. https://bioinfogp.cnb.csic.es/tools/venny/index.html).

Cell cycle

The analysis was performed using the FITC-BrdU Flow Kit (BD Biosciences, Cat. #559619), according to the manufacturer's protocol. In overview, BrdU solution was carefully added directly to Lockés solution, and incubated for 1 h at 37 °C. fixed and permeabilised with a BD Cytofix/Cytoperm buffer for 30 min at room temperature, and treated with 300 µg/mL DNase for 1 h at 37 °C to expose BrdU-labelled DNA. Cells were subsequently stained with FITC-conjugated anti-BrdU antibody for 20 min, and with 7-AAD dye for 15 min, both at room temperature. The analysis was performed on an Accuri™ C6 flow cytometer using BD Accuri™ C6 software (BD Biosciences, Franklin Lakes, NJ, USA).

Apoptosis

We used Nicoletti stain, a classical method for apoptosis detection. This method is based on a selective stain of DNA with Propidium Iodide (PI) and analysis by flow cytometer. Briefly, after different experimental treatments, the cells were washed with Locke solution and resuspended in a PI hypotonic solution (0.1 % sodium citrate (wt/v), 1 % Triton X-100 (v/v) and PI (50 µg/ml Sigma-Aldrich; CAS:25535–16-4)) and incubated 30 min in the dark at room temperature. The analysis was performed on an Accuri™ C6 flow cytometer with 488 nm laser and 610/20 nm detector using BD Accuri™ C6 software (BD Biosciences, Franklin Lakes, NJ, USA).

Western blot

Mitofilin/Mic60 was detected by Western blot analysis. In short, the lysed samples from cells in different conditions (control, MPP+, IGF-II-MPP+, IGF-II) were centrifuged at 300 g for 5 min at 4 °C, supernatants were collected, and protein was measured using a Nanodrop ND-1000/10S UV–VIS spectrophotometer (Thermo Fisher Scientific, Waltham, MA, USA). The proteins (50 μg per well), with a mixture of Laemmli buffer and β-mercaptoethanol, were heated at 95 °C for 5 min and electrophoresed using 4–15 % Mini-PROTEAN® TGX™ precast gels, as per the standard procedure and manufacturer's instructions (Bio-Rad Laboratories, Hercules, CA, USA). After electrophoresis, proteins were transferred to 0.2 μm nitrocellulose membranes using a Trans-Blot Turbo Transfer System (Bio-Rad Laboratories, USA). The membranes were blocked in 5 % fat free milk dissolved in Tris buffer saline -Tween (TBST) for 1 h at room temperature and incubated overnight at 4 °C with the following specific primary antibodies diluted in TBST/5% fat free milk: rabbit anti-β-actin at 1/1500 dilution (from Cell Signaling Technology, USA) and rabbit anti-mitofilin at 1/2000 dilution (Prointech Group, USA). Next, goat anti-rabbit IgG HRP-conjugated at 1/1500 dilution (Bio-Rad Laboratories, USA) in the same buffer, and SuperSignal™ West Pico PLUS chemiluminescent substrate (Thermo Fisher, USA), following the instructions provided by the supplier, was used to visualise protein bands. All membranes were washed three times for 5 min in TBST between each stage. Protein-specific signals were detected by chemiluminescence using a ChemiDoc™ XRS + Imaging System (Bio-Rad Laboratories, USA) and quantification of band intensities was carried out with Image Lab™ Software (Bio-Rad Laboratories, USA).

Measurement of enzyme activity

After the various treatments, cells were homogenised in ice-cold Tris-HCl buffer pH 7.4 with 0.01 % digitonin, followed by centrifuging (5 min, 4 °C, 2000 g) to remove cell debris. The supernatant was used to measure enzymatic activity and protein concentration using Bradford assay.

The measurement of succinate dehydrogenase (EC 1.3.5.1) (SDH) activity was performed using a Cobas Mira autoanalyser at 600 nm and 37 °C in presence of succinate solution that catalyses its oxidation to fumarate and carries electrons from Coenzyme Q2 following the methodology already described [30,31]. One unit of SDH activity represented the oxidation of 1 μmol of succinate in 1 min at 37 °C.

Immunocytochemistry

Before seeding, sterile glass coverslips were placed on the bottom of the wells of 12-well plates and pre-coated with 100 μg/mL of poly-D-lysine (Sigma). After treatments, the fixed cells (methanol −20 °C for 20 min) were incubated with two primary antibodies overnight at 4 °C diluted in PBS/3% BSA: anti p- Checkpoint kinase 1 (Chk1) at 1/1700 dilution (Cell Signaling Technology, USA) and anti-mitofilin at 1:150 dilution (Proteintech). After incubation with primary antibodies, coverslips were incubated with secondary antibody (Alexafluor™ 488 goat anti-mouse (2 drops/mL, Thermo Fisher Scientific, USA) and 4,6-Diamidino-2-phenylindole (DAPI) at 1:1000 dilution for 1 h at room temperature in the dark. Fluoromount (Sigma-Aldrich) was used for the mounting of slides. In the experiments regarding mitofilin, before fixation, cells were dyed with the mitochondrial marker MitoTracker Deep Red FM (MTR) (Molecular Probes, Invitrogen) (30 min at 37 °C). Anti-mouse Alexafluor™ 488, MTR and DAPI were excited by laser light at 405 and 641 nm wavelength.

All the images were acquired using the confocal microscope system LEICA Stellaris 8 (Wetzlar, Germany) and analysed by using LAS AF Lite software (Leica Microsystems AG, Wetzlar, Germany). The co-localisation index of mitofilin was calculated as green over red fluorescence ratio per cell. CHK1 quantification was expressed as fluorescence intensity arbitrary units (AU) per cell. Both co-localisation and quantification were measured using ImageJ software [3].

Statistical analysis

GraphPad software (GraphPad Prism 9.4.1.681 Serial number: GPS-1321494-L###-##### Machine ID: 9D691B583EA licensed to Malaga University) was used for statistical analysis. The statistical tests applied were one-way ANOVA followed by the post-hoc Newman-Keuls multiple comparison test when comparing three or more groups and T-Student when comparing only two groups. Statistical significance was set at $p < 0.05$. For data in which the measured units were arbitrary, the values represent the percentage relative to the control value.

Results and discussion

We have recently shown the neuroprotective effect of IGF-II against oxidative damage [3,17,23]. This study confirms that continuous presence of IGF-II in the medium is essential for its antioxidant protective effect, as it is observed that when removing IGF-II from the medium after the damage is induced, cells do not fully recover to control levels (Figure S1). Furthermore, it shows that in a mice model of PD based in the administration of MPTP, IGF-II can stop the oxidative damage induced by the toxin but does not revert it. This could be due to the fact that living neurons do not behave like the cells in culture [3,16]. The mechanism underlying this effect is mediated by different factors and is mainly focused on the maintenance of mitochondrial structure and oxidative balance [23] improving cell cycle dysregulation and reducing the number of apoptotic cells [32].

Proteomic analysis

Proteomics is the complete evaluation of the structure and function of proteins [33] that could provide a comprehensive map of proteins interactions linked with the neuroprotective effect of IGF-II.

A proteomic analysis was performed of treated cells (*i.e.,* MPP^+, MPP^++IGF-II and IGF-II) compared to control cells. In total, 627 different proteins were identified, with 1 % false discovery rate (Table S1). 503 were identified in the control cells, 515 in MPP^+, 471 in MPP^++ IGF-II cells and 510 in IGF-II group. The Venn diagram highlights 382 proteins common among all experimental conditions, whereas 32, 28, 12 and 24 polypeptides were "unique" for control, MPP^+, MPP^++IGF-II and IGF-II, respectively (Figure S2A). To reveal the differential expressed proteins (DEPs), a MS-based label-free quantification was performed on the 382 common proteins [24]. Each group of treated cells was compared to control cells, and only proteins with a $\log_2$ fold change of ±1 were considered DEPs. In this protein group, the "unique" proteins found in each experimental condition were added. The results obtained indicate that MPP^+, MPP^++IGF-II treatment and IGF-II, compared to control cells, modified the expression of 197 proteins (*i.e.,* 95 and 102 proteins were respectively up- and down-regulated) 246 proteins (*i.e.,* 121 and 125 proteins were respectively up- and down-regulated) and 207 proteins (*i.e.,* 116 and 91 proteins were respectively up- and down-regulated) (Figure S2B and Table S2).

For DEPs, a gene ontology (GO) enrichment analysis was performed to describe the biological processes, cellular components, and molecular functions of these proteins (Table S3).

The cells treated with MPP^+, compared to control cells, showed an over-expression of proteins involved in nucleosome assembly, replication and in proteasome, a multi-subunit enzyme complex that plays a key role in the regulation of proteins controlling cell-cycle progression and apoptosis [34,35]. Moreover, proteomic analysis identified all six minichromosomal maintenance proteins (*i.e.*, Mcm 2–7) being some of them (*i.e.*, Mcm2; Mcm4 and Mcm5) were down-regulated in MPP^+. This Mcm complex is a protein family necessary for the initiation and progression of DNA replication in the cell cycle, and their expression is correlated with the cellular proliferative status [36]. The effect on their expression could be an early or an acute response to MPP^+ determining an interruption of cell proliferation in these cells [37]. Interestingly, in the same cells, the relative composition of the 26S proteasome complex appeared to be modified compared to control cells (Table S2) and modulated by IGF-II. Both an increase and a decrease in proteasome abundance, and/or an altered assembly can lead to intracellular protein accumulation, a pathological feature of some neurodegenerative diseases, such as PD [38–41]. The IGF-II would act on this effect throughout the modulation of cellular proliferative processes [19,20,42,43] and proteasome processing [44–47], although deeper studies would be necessary to assess this point specifically.

The treatment with the combination of IGF-II and MPP^+ led to a biological process enrichment in fumarate and in glutamic/aspartic metabolic processes compared to control cells (Table S3). Moreover, it has previously been proved that GOT1 down-regulation (aspartate aminotransferase) is a key metabolic gene in Alzheimer's and Parkinson's disease [48]. Interestingly, fumarate is an intermediate metabolite of the tricarboxylic acid cycle obtained from succinate, in a reaction catalysed by succinate dehydrogenase (SDH) and converted to L-malate by fumarate hydratase in mitochondria [49]. The proteomic results of this study (Tables S1 and S2) show an up- and down-regulation of SDHA subunit and fumarate hydratase respectively, in accordance with IGF-II stimulus, which can compensate the inhibitory effect of MPP^+ on complex I and II [3,50,51], maintaining the rate of tricarboxylic acid cycle [52]. The effect of IGF-II could be mediated by the increase in Nrf2 described by our group and others [3,53,54]. To determine if the changes found in proteomic in SDHA subunit level interfere with the enzyme activity, we measured SDH activity by spectrophotometric enzyme assay (Figure S3). MPP^+ treatment induced a significant reduction of the enzyme activity compared to control cells that was recovered in the presence of IGF-II. Interestingly, we have found a decrease in SDH activity in presence of MPP^+ compared to control cells without a decrease in proteomic levels of SDHA subunit, this could be due to post-translational modifications (*e.g.,* phosphorylation) which it has been demonstrated to regulate complex II activity [55]; again, more deep studies would be necessary to clarify this point specifically.

Moreover, an up-regulation of mitofilin, a protein essential for maintaining mitochondrial morpho-functionality [56,57] and involved in Parkinsońs disease pathogenesis [56,57]. In this study, ultrastructural analysis has demonstrated that the presence of IGF-II protected mitochondria from MPP^+ toxicity, and this could be due to an increase in the mitofilin level shown below.

In IGF-II vs control cells, the DEPs were significantly enriched for transcription and translation. These findings agree with previous studies demonstrating that IGF-II stimulates transcription and protein synthesis by phosphorylation of FOXO and mTOR [3]. However, the transcription and translation processes require an energy supply, supported by the up-regulation of metabolic processes such as glycolysis. In support of this, an up-regulation of phosphofructokinase (ATP-dependent 6-phosphofructokinase), a limiting enzyme of glycolysis, was found. Moreover, GO analysis (Table S3) revealed a rise in the proteasome complex, which is probably involved in removal of misfolded protein or protein aggregates, thus preventing cell damage [46,58].

Mitochondrial ultrastructure and function

Ultrastructural analysis reveals that IGF-II attenuates the deleterious mitochondrial effects induced by MPP^+. Untreated cells (*i.e.*, control cells) showed the presence of many mitochondria surrounding the nucleus and the mitochondria membranes, and mitochondrial cristae were found to be well-organised (Fig. 1A arrows). In MPP^+-treated cells, many mitochondria showed clear signs of damage, such as reduced matrix density, destroyed cristae architecture and swelling; their number per cell was also reduced, confirming previous data [3] (Fig. 1B arrows). Cells treated with both MPP^+ and IGF-II showed an improvement in mitochondrial morphology, with the majority of mitochondria/cell displaying intact outer and inner membranes and preserved cristae (Fig. 1C arrows).

The analyses of mitochondrial size parameters highlighted a significant increase of mitochondrial area and perimeter in MPP^+ treated cells compared to control cells, confirming TEM observations (Fig. 1 table). The values of aspect ratio and roundness were similar in control and treated cells (*i.e.,* MPP^+, MPP^++IGF-II). Circularity was significantly increased in all treated groups, whereas changes in form factor was significant only in MPP^+-treated cells. All the ultrastructural analyses together indicate that IGF-II treatment can reduce the deleterious effects induced by MPP^+ and related to mitochondrial function [59].

Related to the structural changes seen in mitochondria and detected by proteomic analyses (Table S2), as commented above, this study also considered mitofilin. The immunocytochemistry images obtained in the study showed a co-localisation of mitofilin and mitochondria (Fig. 2A), as this protein is anchored to the inner membrane [60]. We have found a statistically significant reduction of co-localisation index in cells treated with MPP^+ vs CO cells, which points to a de-co-localisation of mitofilin in mitochondria inducing mitochondrial dysfunction. Co-administration of IGF-II reversed this situation. In the presence of BMS to inhibit IGF-I and insulin receptors, the co-localisation index decreases compared to MPP^++IGF-II treated cells, supporting the interaction of IGF-II with other receptors than IGF-IIr as responsible for this effect (Fig. 2A). Also, mitofilin expression was measured by Western blot (Fig. 2B), where a decrease (16 %) in its levels in MPP^+ treated cells was found, whereas IGF-II increased the levels of mitofilin by 10 % compared to control cells, although neither variation reached statistical significance. Interestingly, IGF-II increased the levels of mitofilin by 26 % compared to MPP^+-treated cells ($p < 0.05$), more in-depth studies would be necessary to further clarify this point. This decrease in mitofilin may be due to increased oxidative damage produced by MPP^+, as previously shown [3]. The decrease in mitofilin could be responsible for modifications in the cell cycle, which in turn would increase cell death by apoptotic processes [61] (see below). IGF-II promotes mitochondrial integrity by recovering the amount and location of mitofilin in mitochondria (Fig. 2), re-establishing mitochondrial redox homeostasis and function (Fig. 3).

In order to study mitochondrial function, the basal OCR, ATP production, proton leak, maximal respiratory capacity and SRC were measured in control, in MPP^+ and IGF-II + MPP^+ treated cells (Fig. 3). The study found a 28 % decrease in basal OCR in MPP^+-treated cells compared to control, and incubation of MPP^+-treated cells in the presence of IGF-II reduces the OCR decrease to only 13 %, showing a protective effect against the damage

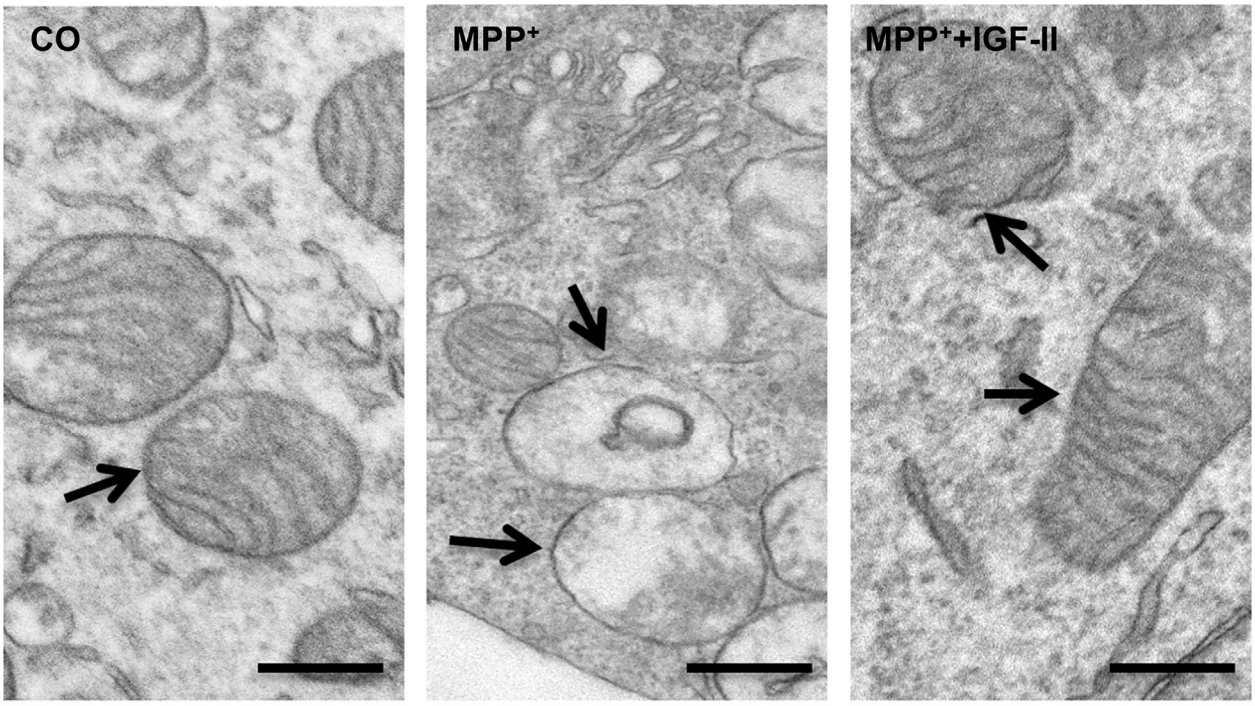

Mitochondrial size and shape descriptors	CO	MPP+	MPP+IGF-II
Mitochondrial area (μm²)	0.31 ± 0,01	0.39 ± 0.02*	0.28 ± 0.01
External perimeter (μm)	2.08 ± 0.03	2.29 ± 0.04*	1.96 ± 0.05
Aspect ratio (AU)	1.28 ± 0.02	1.24 ± 0.02	1.29 ± 0.02
Circularity (0 - 1) (AU)	0.87 ± 0.004	0.90 ± 0.005*	0.89 ± 0.005*
Roundness (0 - 1) (AU)	0.80 ± 0.01	0.82 ± 0.02	0.80 ± 0.01
Form factor (AU)	1.15 ± 0.02	1.11 ± 0.01*	1.13 ± 0.005

Fig. 1. Representative transmission electron microscopy (TEM) images of mitochondria in untreated cells (CO) or cells treated with MPP^+ or MPP^++IGF-II. Scale bar: 500 nm. Table below shows morphological parameters of mitochondria analysed on TEM images. Data are expressed as mean ± SEM. *p < 0.05 vs CO. The analyses were performed on 100 mitochondria for each experimental group using Image J software.

induced by MPP^+ (Fig. 3B). Regarding ATP production, in cells treated with MPP^+, a 30 % decrease in ATP production was found compared to control cells; again, IGF-II protects cells from MPP^+ damage, limiting ATP production to a decrease of only 11 % compared to control cells (Fig. 3C). Similarly, maximal respiratory capacity and SRC decrease in MPP^+-treated cells (24 % and 18 % compared to control respectively) and again are recovered when incubated in the presence of IGF-II (10 % and 3 % of decrease compared to control respectively) (Fig. 3E and F respectively). Conversely, proton leak decreases by 25 % in cells treated with MPP^+ without any recovery seen when incubated in the presence of IGF-II (Fig. 3D). The findings of this study on the toxic effect of MPP^+ on OCR, ATP production, proton leak, maximal respiratory capacity and SRC in treated cells agree with other authors [62,63]. With the exception of proton leak, IGF-II avoids the damage induced by MPP^+ in all studied parameters agreeing with previous results from our group [23]. The protective effect found for IGF-II could be due to the recovery of ATP production, along with the recovery of OCR; also, IGF-II recovers the damage on SCR allowing mitochondria to produce more energy when needed and restore mitochondrial homeostasis, agreeing with previous results [3,23]. When these experiments were performed in the presence of BMS, the inhibitor of insulin and IGF-I receptor, the effect of IGF-II was maintained, indicating that the effect of this hormone is mediated through its specific IGF-II receptor (Fig. 3). Furthermore, the involvement of the specific IGF-II receptor in these effects has also been previously demonstrated by our group [3] using the selective agonist LEU[27]IGF-II, where we found almost identical effects on mitochondrial function and ROS production in both, IGF-II and LEU[27]IGF-II treated cells.

Finally, it has to be highlighted that no changes were observed compared to control cells in those treated only with IGF-II (Figures S4 and S5), so the effects are only present when damage has been produced, in this case by MPP^+.

The mechanism by which IGF-II induce these effects could be related to the above-mentioned recovery on the amount and loca-

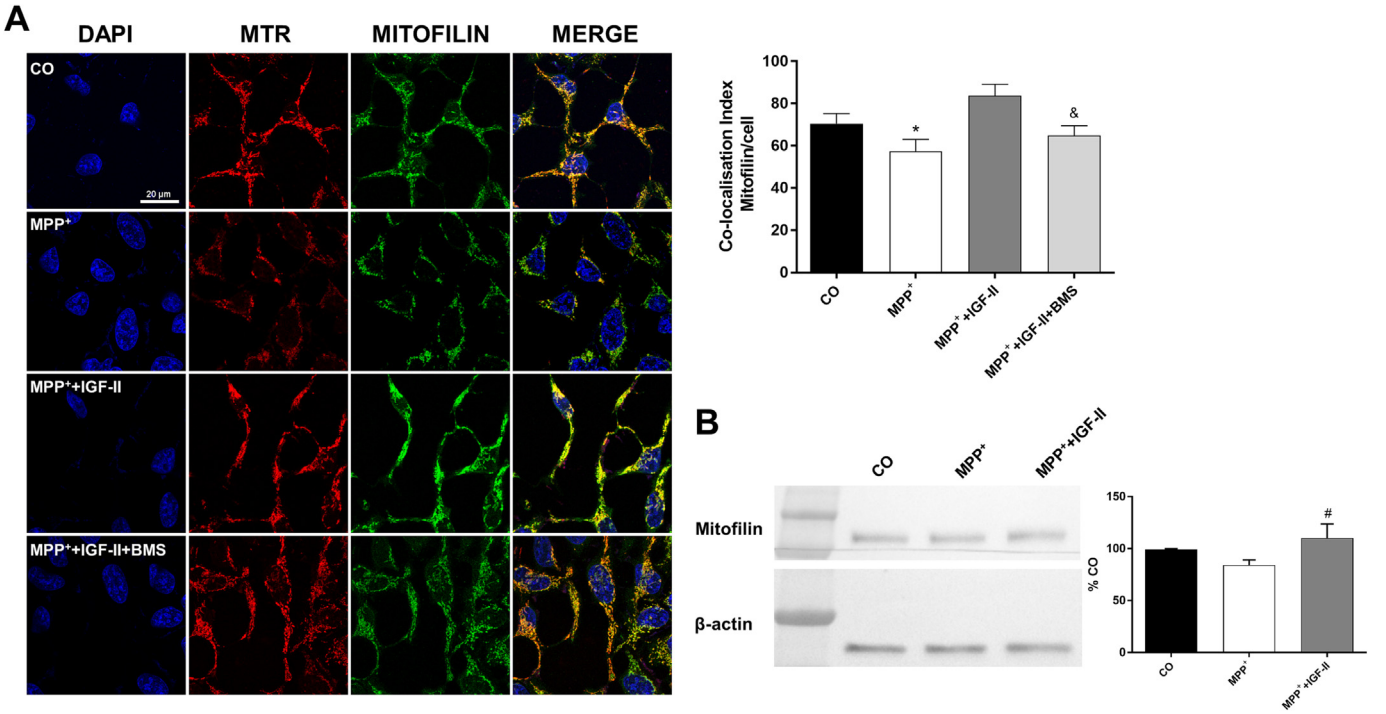

Fig. 2. A) Representative immunocytochemistry of mitofilin expression and colocalization index, calculated as green over red fluorescence ratio per cell, in untreated cells (CO) or cells treated with MPP^+, MPP^++IGF-II or MPP^++IGF-II + BMS. The analyses were performed on 50 cells for each experimental group, using Image J software. **B)** Representative western blot and quantification after normalising with β-actin; data were combined from 3 to 4 independent experiments and presented as mean ± SEM (*p < 0.05 vs CO, #p < 0.05 vs MPP^+,&p < 0.05 vs MPP^++IGF-II). (For interpretation of the references to colour in this figure legend, the reader is referred to the web version of this article.)

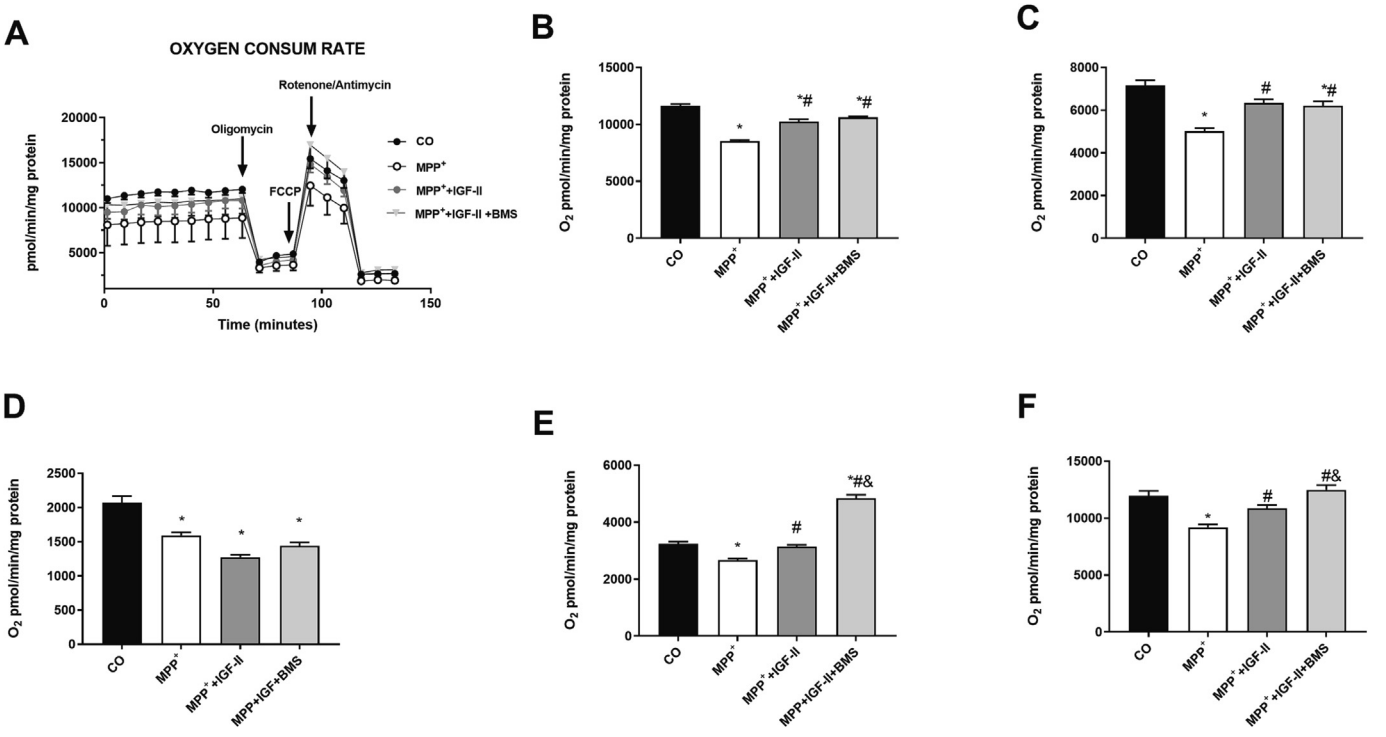

Fig. 3. A) Oxygen consumption rate time course (OCR); **B)** Basal situation, assessed after two hours of the first treatment period; **C)** ATP production; **D)** Proton leak; **E)** Spare respiratory capacity (SRC); and **F)** Maximal respiration. Values represent mean ± SEM of at 5 to 6 experiments per situation performed in triplicate. (*p < 0.05 vs CO, #p < 0.05 vs MPP^+, &p < 0.05 vs MPP^++IGF-II).

tion of mitofilin in mitochondria, a protein involved in mitochondrial crista morphology and function; these mitofillin protective effects have also been seen in other mitochondrial functional studies [56,61,64]. Also, this increase in mitochondrial function (ATP

production and OCR) provides enough energy to promote the G_2/M change to continue the normal cell cycle [65] as shown in the experiments on the cell cycle.

Cell cycle analysis and apoptosis

As shown in proteomic studies, both MPP$^+$ and IGF-II modulate protein expression involved in the cell cycle. Fig. 4A shows a representative plot of BrdU/7-AAD cell cycle analysis and the percentage of cells in sub-G_1, G_0/G_1, S and G_2/M phases.

G_0/G_1 and S phases were found to be decreased by 1.6-fold and 1.3-fold respectively in MPP + -treated cells compared to control. In opposition, the proportion of cells in the G_2/M phase significantly increased (5-fold) compared to control after treatment with MPP$^+$, as previously described, meaning a G_2/M arrest [66]. IGF-II counteracts the damage caused by MPP$^+$ promoting the G2/M cell cycle progression. Furthermore, we have performed apoptosis experiment in which MPP$^+$ produces a statistically significant increase in apoptosis compared to control cell. The inclusion of IGF-II in the incubation media decreases apoptosis and this effect is mediated exclusively by the IGF-IIr as we did not see differences when the insulin and IGF-I receptors were blocked with BMS; also, the apoptosis returns to values similar to those of MPP$^+$ when the IGF-IIr was blocked with the antibody against it (AB) (Fig. 4B). Furthermore, the involvement of the specific IGF-II receptor in these effects has also been previously demonstrated by our group [3] using the selective agonist LEU[27]IGF-II, where we found almost identical effects on cell death, in both IGF-II and LEU[27]IGF-II treated cells.

In the cell cycle analysis, it was shown that a significant number of MPP$^+$-treated cells entered the cell cycle and duplicated their nuclear DNA. Moreover, MPP$^+$ treatment induced an important increase in the number of apoptotic cells, as also previously reported [66], while IGF-II demonstrated to reduce both cell cycle entry and apoptosis (Fig. 4). All together, the results suggest that apoptotic death is a consequence of entry into the cell cycle and the arrest of G_2/M as a consequence, at least partially, of a decrease in mitofilin. Several studies have provided evidence that cell-cycle activation may play a key role in neuronal apoptosis [32,66,67] and mitosis and apoptosis are highly conserved mechanisms that share molecular mediators and are activated concomitantly [68,69]; therefore, the prevention of neurons from entering the cell cycle or delaying entry could have a neuroprotective role [7,69]. Which could be the effect of IGF-II. This may be associated to the increase in mitochondrial function (ATP production and OCR) as we previously showed in this work. Finally, it has to be highlighted that no changes in cell cycle and apoptosis were observed compared to control cells in those treated only with IGF-II (Figures S6A and B, respectively), so all effects are produced only when damage is induced; in this case by MPP$^+$.

Another important factor in the regulation of the cell cycle is Chk1, an enzyme that phosphorylates downstream effectors to trigger a pleiotropic response that includes energy consumption, transcription regulation, cell-cycle arrest or delay, DNA repair, or cell death if the injury is too heavy to be repaired [70]. After its activation by phosphorylation, Chk1 induces cell-cycle delay and/or blocks replication (in G_2 or S phases) when DNA is damaged [71,72]. In this study, Chk1 expression was assessed by immunocy-

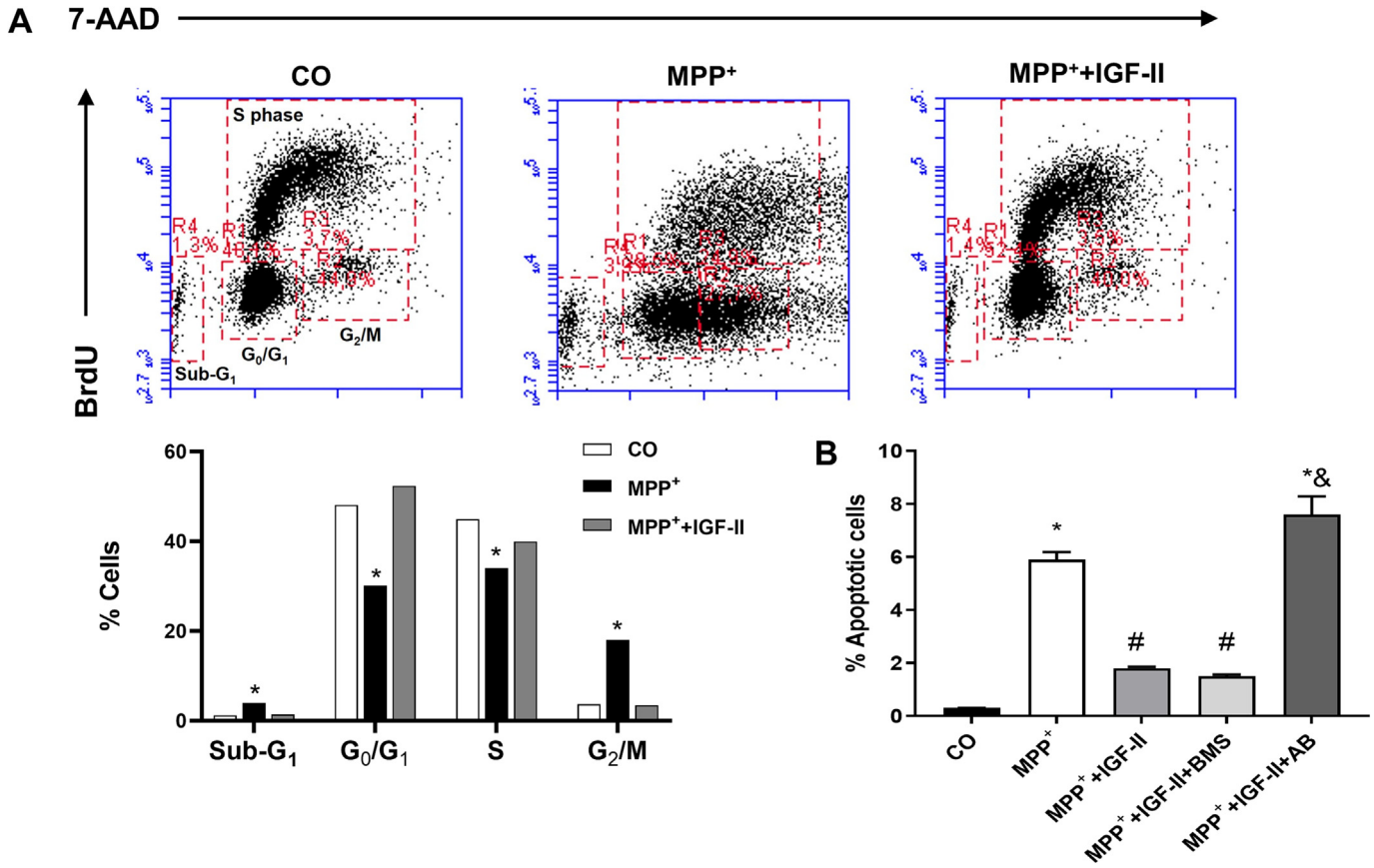

Fig. 4. A) Representative plot of by flow cytometry of BrdU/7AAD cell cycle in untreated cells (CO) or cells treated with MPP $^+$or MPP$^+$+IGF-II and analysis of percentage of different subpopulations of the cell cycle. **B)** Percentage of apoptotic cells after different treatments. Values represent the mean ± SEM of at 4 to 5 experiments per situation (* $p < 0.05$ vs CO, # $p < 0.05$ vs MPP$^+$, &$p < 0.05$ vs MPP$^+$+IGF-II).

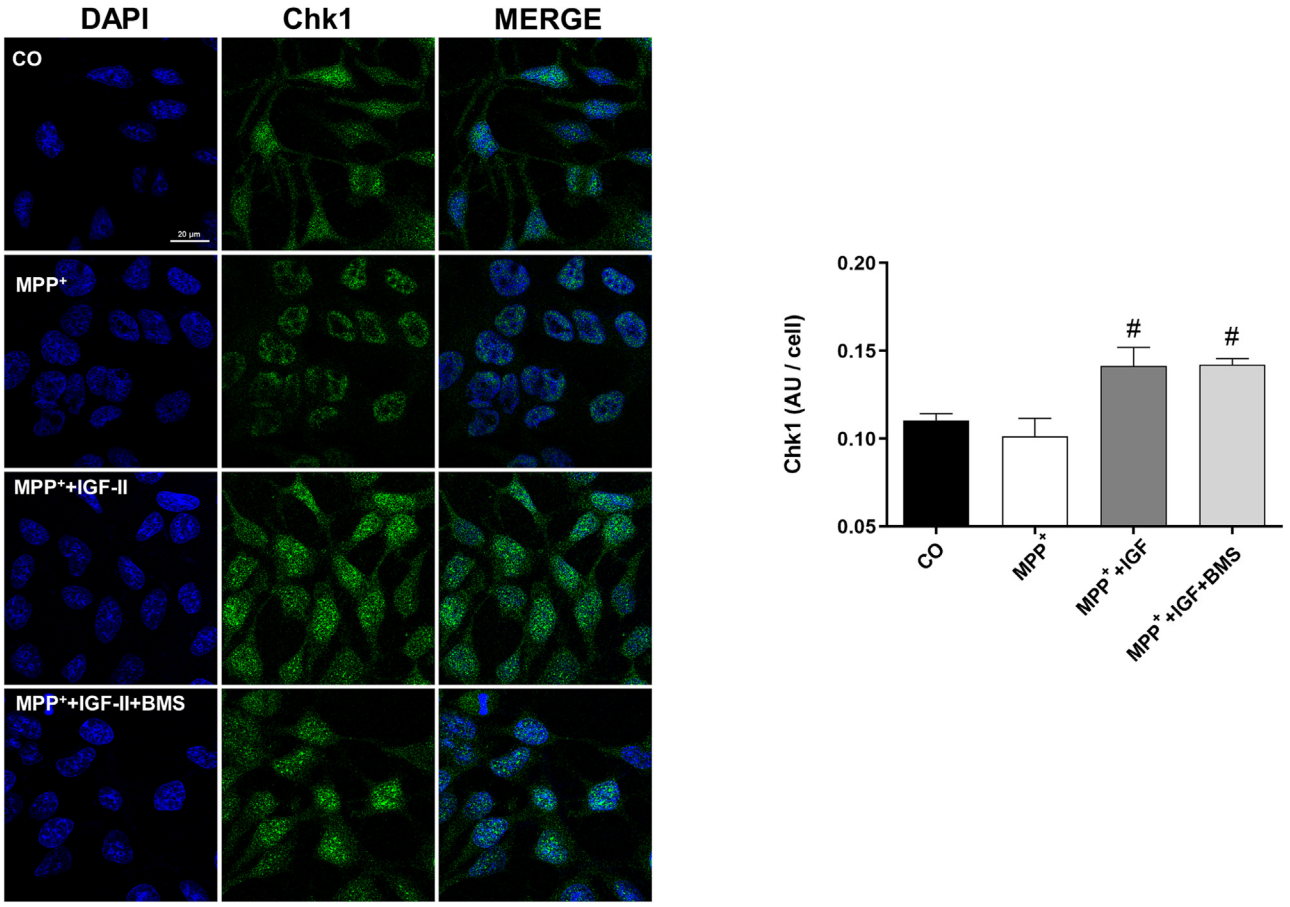

Fig. 5. Immunocytochemistry of Chk1 expression and quantification of immunofluorescence levels in untreated cells (CO) or cells treated with MPP^+, MPP^++IGF-II or MPP^++IGF-II + BMS. The analyses were performed on 50 cells for each experimental group, using Image J software. (#$p < 0.05$ vs MPP^+). Values represent the mean ± SEM of at 4 to 5 experiments per situation.

tochemistry (Fig. 5); administering MPP^+ produce no statistically significant changes in the expression of Chk1 (10 % less than control). The addition of IGF-II in the incubation media leads to a statistically significant increase in the expression of Chk1, close to 30 %, compared to control cells. This effect could be attributed to the specific interaction between IGF-II and its specific IGF-IIr, as the blocking of insulin and IGF-I receptors by BMS does not produce any change in the percentage of increase of Chk1 caused by IGF-II. On the other hand, distribution of Chk1 within the nucleus differs between the situations studied; immunofluorescence images show that Chk1 expression was near nuclear membrane in cells treated with MPP^+, maybe associated with condensed chromatin due to cellular apoptotic processes. Instead, in cells that were co-administered with IGF-II or were not treated (control cells), it was located throughout the nucleoplasm. The increase in Chk1 expression after IGF-II treatment found in this study could be interpreted as a neuroprotective response to prevent damage from neurotoxic agents based on the ability to interfere with the cell cycle (death and/or division) [70,73,74]. Some studies have also postulated that Chk1 inhibition could be neuroprotective in some neurodegenerative diseases, such as Alzheimeŕs disease [75], although there are some discrepancies depending on the type of neurone involved (embryo or adult) [76]. The neuroprotective effect of IGF-II could also be attributed to the increase in Chk1 levels that in turn would phosphorylate SOD [77], preventing further DNA oxidative damage, in accordance with previous results from our group [17]. Again, the results obtained in control cells treated only with IGF-II showed no change in cell cycle and expression of Chk1 compared to untreated cells (Figure S6C), supporting the idea that the effects of this hormone are induced only by its interaction with MPP^+.

Limitations

This study was performed in a cellular model based on a substantia nigra embryonic cell line, and not in adult cells, so, some differences could arise when compared with adult cells. Furthermore, all the experiments were performed in the absence of antioxidants and protective factors in the incubation medium, which is necessary to obtain accurate results concerning the IGF-II/IGF-IIr effects, but it does not simulate real physiological conditions for the cells.

Our results suggested that the neuroprotective effects of IGF-II are mediated by IGF-IIr, but it cannot be ruled out its interaction with other receptors (*i.e.*, Insulin and IGF-I receptors), which should be analysed in further studies.

Conclusions

In our experiments, IGF-II stimulates cellular mechanisms to protect DNA integrity, as shown by the increase of Chk1 found when IGF-II is present in the incubation medium. Besides, IGF-II also improves mitochondrial function by promoting mitofilin association with mitochondria, recovering function and redox home-

ostasis, avoiding ROS formation and maintaining integrity and function of proteins; this would result in a regulation of transcription factors decreasing apoptosis and cell death induced by MPP^+. Furthermore, all these antioxidant and protective effects are mediated mainly by the interaction of IGF-II with IGF-IIr and are due to its continuous presence in the medium.

CRediT author contribution statement

M.G-F, E.M-M, J.P and B.G conceptualization. M.G-F, E.M-M, and SY. R-Z Funding acquisition. F.B and FD. L (electronic microscopy and proteomic analyses); E. M-M, E.L, S.G, N.V, SY. R-Z and P.Z-G (cell-cycle analyses, western blot and immunocytochemistry) Methodology and Investigation. M.G-F, E.M-M, N.V, and SY R-Z Formal analysis and visualization. J. P, M.G-F, E. M-M. and B.G. writing – review & editing

Declaration of competing interest

The authors declare that they have no known competing financial interests or personal relationships that could have appeared to influence the work reported in this paper.

Acknowledgments

We wish to thank Dr. Ernest Arenas for providing SN4741 cells and Lilly Laboratories for providing IGF-II cells. This research was supported by the following projects: M.G-F, E.M-M and SY.R-Z Plan Propio de la Universidad de Málaga 2022 (B4-2023-3, B1-2022-15 and C1) and Ministerio de Economía y Competitividad. Gobierno de España. (MINECO, Agencia Estatal de Investigación cofinanciado por FEDER-UE (PID2020-113806RB-I00) and; F.B "Fondazione Cassa di Risparmio di Modena" for funding use expenses of Talos F200S G2 transmission electron microscope and Q Exactive Hybrid Quadrupole-Orbitrap Mass Spectrometer at CIGS, UNIMORE. Partial funding for open access charge: Universidad de Málaga / CBUA.

Appendix A. Supplementary data

Supplementary data to this article can be found online at https://doi.org/10.1016/j.jare.2024.01.036.

References

[1] Tysnes OB, Storstein A. Epidemiology of Parkinson's disease. J Neural Transm 2017;124:901–5. doi: https://doi.org/10.1007/s00702-017-1686-y.
[2] Jankovic J, Tan EK. Parkinson's disease: Etiopathogenesis and treatment. J Neurol Neurosurg Psychiatry 2020;91:795–808. doi: https://doi.org/10.1136/jnnp-2019-322338.
[3] Martín-Montañez E, Valverde N, Ladrón de Guevara-Miranda D, Lara E, Romero-Zerbo YS, Millon C, et al. Insulin-like growth factor II prevents oxidative and neuronal damage in cellular and mice models of Parkinson's disease. Redox Biol 2021;46. doi: https://doi.org/10.1016/j.REDOX.2021.102095.
[4] Son JH, Chun HS, Joh TH, Cho S, Conti B, Lee JW. Neuroprotection and neuronal differentiation studies using substantia nigra dopaminergic cells derived from transgenic mouse embryos. J Neurosci 1999;19:10–20. doi: https://doi.org/10.1523/JNEUROSCI.19-01-00010.1999.
[5] Barnham KJ, Masters CL, Bush AI. Neurodegenerative diseases and oxidative stress. Nat Rev Drug Discov 2004;3:205–14. doi: https://doi.org/10.1038/nrd1330.
[6] Wang Y, Xu E, Musich PR, Lin F. Mitochondrial dysfunction in neurodegenerative diseases and the potential countermeasure. CNS Neurosci Ther 2019;25:816–24. doi: https://doi.org/10.1111/cns.13116.
[7] Joseph C, Mangani AS, Gupta V, Chitranshi N, Shen T, Dheer Y, et al. Cell cycle deficits in neurodegenerative disorders: Uncovering molecular mechanisms to drive innovative therapeutic development. Aging Dis 2020;11:946. doi: https://doi.org/10.14336/AD.2019.0923.
[8] Requejo-Aguilar R. Cdk5 and aberrant cell cycle activation at the core of neurodegeneration. Neural Regen Res 2023;18:1186. doi: https://doi.org/10.4103/1673-5374.360165.
[9] Martínez-Cué C, Rueda N. Cellular senescence in neurodegenerative diseases. Front Cell Neurosci 2020;14:16. doi: https://doi.org/10.3389/fncel.2020.00016.
[10] Stern SA, Kohtz AS, Pollonini G, Alberini CM. Enhancement of memories by systemic administration of insulin-like growth factor II. Neuropsychopharmacology 2014. doi: https://doi.org/10.1038/npp.2014.69.
[11] Ziegler AN, Levison SW, Wood TL. Insulin and IGF receptor signalling in neural-stem-cell homeostasis. Nat Rev Endocrinol 2015;11:161–70. doi: https://doi.org/10.1038/nrendo.2014.208.
[12] Beletskiy A, Chesnokova E, Bal N. Insulin-Like Growth Factor 2 as a possible neuroprotective agent and memory enhancer—Its comparative expression, processing and signaling in mammalian CNS. Int J Mol Sci 2021;22:1849. doi: https://doi.org/10.3390/ijms22041849.
[13] Werner H, LeRoith D. Insulin and insulin-like growth factor receptors in the brain: Physiological and pathological aspects. Eur Neuropsychopharmacol 2014;24:1947–53. doi: https://doi.org/10.1016/j.euroneuro.2014.01.020.
[14] Alberini CM. IGF2 in memory, neurodevelopmental disorders, and neurodegenerative diseases. Trends Neurosci 2023;46:488–502. doi: https://doi.org/10.1016/j.tins.2023.03.007.
[15] Castilla-Cortazar I, Garcia-Fernandez M, Delgado G, Puche JEE, Sierra I, Barhoum R, et al. Hepatoprotection and neuroprotection induced by low doses of IGF-II in aging rats. J Transl Med 2011;9:103. doi: https://doi.org/10.1186/1479-5876-9-103.
[16] Martín-Montañez E, Millon C, Boraldi F, Garcia-Guirado F, Pedraza C, Lara E, et al. IGF-II promotes neuroprotection and neuroplasticity recovery in a long-lasting model of oxidative damage induced by glucocorticoids. Redox Biol 2017;13:69–81. doi: https://doi.org/10.1016/j.redox.2017.05.012.
[17] Martin-Montañez E, Pavia J, Santin LJ, Boraldi F, Estivill-Torrus G, Aguirre JA, et al. Involvement of IGF-II receptors in the antioxidant and neuroprotective effects of IGF-II on adult cortical neuronal cultures. Biochim Biophys Acta Mol Basis Dis 2014;1842:1041–51. doi: https://doi.org/10.1016/j.bbadis.2014.03.010.
[18] Steinmetz AB, Stern SA, Kohtz AS, Descalzi G, Alberini CM. Insulin-like growth factor II Targets the mTOR pathway to reverse autism-like phenotypes in mice. J Neurosci 2018;38:1015–29. doi: https://doi.org/10.1523/JNEUROSCI.2010-17.2017.
[19] Pardo M, Cheng Y, Sitbon YH, Lowell JA, Grieco SF, Worthen RJ, et al. Insulin growth factor 2 (IGF2) as an emergent target in psychiatric and neurological disorders. Review Neurosci Res 2019;149:1–13. doi: https://doi.org/10.1016/j.neures.2018.10.012.
[20] Ouchi Y, Banno Y, Shimizu Y, Ando S, Hasegawa H, Adachi K, et al. Reduced adult hippocampal neurogenesis and working memory deficits in the Dgcr8-deficient mouse model of 22q11.2 deletion-associated schizophrenia can be rescued by IGF2. J Neurosci 2013;33:9408–19, 33/22/9408 [pii]. doi: https://doi.org/10.1523/JNEUROSCI.2700-12.2013.
[21] Pascual-Lucas M, Viana da Silva S, Di Scala M, Garcia-Barroso C, Gonzalez-Aseguinolaza G, Mulle C, et al. Insulin-like growth factor 2 reverses memory and synaptic deficits in APP transgenic mice. EMBO Mol Med 2014;6:1246–62. doi: https://doi.org/10.15252/emmm.201404228.
[22] Hawkes C, Kar S. Insulin-like growth factor-II/mannose-6-phosphate receptor: widespread distribution in neurons of the central nervous system including those expressing cholinergic phenotype. J Comp Neurol 2003;458:113–27. doi: https://doi.org/10.1002/cne.10578.
[23] Claros S, Cabrera P, Valverde N, Romero-Zerbo SY, López-González MV, Shumilov K, et al. Insulin-like Growth Factor II Prevents MPP+ and glucocorticoid mitochondrial-oxidative and neuronal damage in dopaminergic neurons. Antioxidants 2021;11:41. doi: https://doi.org/10.3390/antiox11010041.
[24] Lofaro FD, Boraldi F, Garcia-Fernandez M, Estrella L, Valdivielso P, Quaglino D. Relationship between mitochondrial structure and bioenergetics in Pseudoxanthoma elasticum dermal fibroblasts. Front Cell Dev Biol 2020;8:1532. doi: https://doi.org/10.3389/FCELL.2020.610266.
[25] Gibellini L, De Biasi S, Paolini A, Borella R, Boraldi F, Mattioli M, et al. Altered bioenergetics and mitochondrial dysfunction of monocytes in patients with COVID-19 pneumonia. EMBO Mol Med 2020;12:1–13. doi: https://doi.org/10.15252/emmm.202013001.
[26] Leung DTH, Chu S. Measurement of oxidative stress: mitochondrial function using the seahorse system. Methods Mol Biol 2018;1710:285–93. doi: https://doi.org/10.1007/978-1-4939-7498-6_22.
[27] Brand MD, Nicholls DG. Assessing mitochondrial dysfunction in cells. Biochem J 2011;435:297–312. doi: https://doi.org/10.1042/BJ20110162.
[28] Bradford MM. A rapid and sensitive method for the quantitation of microgram quantities of protein utilizing the principle of protein-dye binding. Anal Biochem 1976;72:248–54. doi: https://doi.org/10.1016/0003-2697(76)90527-3.
[29] Szklarczyk D, Gable AL, Lyon D, Junge A, Wyder S, Huerta-Cepas J, et al. STRING v11: Protein-protein association networks with increased coverage, supporting functional discovery in genome-wide experimental datasets. Nucleic Acids Res 2019;47:D607–13. doi: https://doi.org/10.1093/nar/gky1131.
[30] Ziegler D, Rieske JS. [42] Preparation and properties of succinate dehydrogenase-coenzyme Q reductase (complex II). Oxidation and Phosphorylation, vol. 10, Academic Press; 1967, p. 231–5. https://doi.org/10.1016/0076-6879(67)10045-1.
[31] Munujos P, Collcanti J, Gonzalezsastre F, Gella FJ. Assay of succinate dehydrogenase activity by a colorimetric-continuous method using

iodonitrotetrazolium chloride as electron acceptor. Anal Biochem 1993;212:506–9. doi: https://doi.org/10.1006/abio.1993.1360.
[32] Klein JA, Ackerman SL. Oxidative stress, cell cycle, and neurodegeneration. J Clin Investig 2003;111:785–93. doi: https://doi.org/10.1172/JCI200318182.
[33] Al-Amrani S, Al-Jabri Z, Al-Zaabi A, Alshekaili J, Al-Khabori M. Proteomics: Concepts and applications in human medicine. World J Biol Chem 2021;12:57–69. doi: https://doi.org/10.4331/wjbc.v12.i5.57.
[34] Türker F, Cook EK, Margolis SS. The proteasome and its role in the nervous system. Cell Chem Biol 2021;28:903–17. doi: https://doi.org/10.1016/j.chembiol.2021.04.003.
[35] Adams J. The proteasome: structure, function, and role in the cell. Cancer Treat Rev 2003;29(Suppl 1):3–9. doi: https://doi.org/10.1016/s0305-7372(03)00081-1.
[36] Mei L, Cook JG. Efficiency and equity in origin licensing to ensure complete DNA replication. Biochem Soc Trans 2021;49:2133–41. doi: https://doi.org/10.1042/BST20210161.
[37] Frade JM, Ovejero-Benito MC. Neuronal cell cycle: the neuron itself and its circumstances. Cell Cycle 2015;14:712–20. doi: https://doi.org/10.1080/15384101.2015.1004937.
[38] Suthar SK, Lee S-Y. Truncation or proteolysis of α-synuclein in Parkinsonism. Ageing Res Rev 2023:. doi: https://doi.org/10.1016/j.arr.2023.101978101978.
[39] Bentea E, Verbruggen L, Massie A. The proteasome inhibition model of Parkinson's disease. J Parkinsons Dis 2017;7:31–63. doi: https://doi.org/10.3233/JPD-160921.
[40] Thibaudeau TA, Anderson RT, Smith DM. A common mechanism of proteasome impairment by neurodegenerative disease-associated oligomers. Nat Commun 2018:9. doi: https://doi.org/10.1038/s41467-018-03509-0.
[41] Bi M, Du X, Jiao Q, Chen X, Jiang H. Expanding the role of proteasome homeostasis in Parkinson's disease: Beyond protein breakdown. Cell Death Dis 2021:12. doi: https://doi.org/10.1038/s41419-021-03441-0.
[42] Ferrón SR, Radford EJ, Domingo-Muelas A, Kleine I, Ramme A, Gray D, et al. Differential genomic imprinting regulates paracrine and autocrine roles of IGF2 in mouse adult neurogenesis. Nat Commun 2015;6:8265. doi: https://doi.org/10.1038/ncomms9265.
[43] Zhu X, Yan J, Bregere C, Zelmer A, Goerne T, Kapfhammer JP, et al. RBM3 promotes neurogenesis in a niche-dependent manner via IMP2-IGF2 signaling pathway after hypoxic-ischemic brain injury. Nat Commun 2019;10:1–14. doi: https://doi.org/10.1038/s41467-019-11870-x.
[44] García-Huerta P, Troncoso-Escudero P, Wu D, Thiruvalluvan A, Cisternas-Olmedo M, Henríquez DR, et al. Insulin-like growth factor 2 (IGF2) protects against Huntington's disease through the extracellular disposal of protein aggregates. Acta Neuropathol 2020;140:737–64. doi: https://doi.org/10.1007/s00401-020-02183-1.
[45] Mellott TJ, Pender SM, Burke RM, Langley EA, Blusztajn JK. IGF2 ameliorates amyloidosis, increases cholinergic marker expression and raises BMP9 and neurotrophin levels in the hippocampus of the APPswePS1dE9 Alzheimer's disease model mice. PLoS One 2014;9:e94287. doi: https://doi.org/10.1371/journal.pone.0094287.
[46] Troncoso-Escudero P, Hetz C, Vidal RL. Therapeutic potential of insulin-like growth factor 2 in Huntington's disease: controlling proteostasis to alleviate the load of misfolded protein. Neural Regen Res 2021;16:1564–5. doi: https://doi.org/10.4103/1673-5374.303020.
[47] Wang Y, MacDonald RG, Thinakaran G, Kar S, Kar S. Insulin-Like Growth Factor-II/Cation-Independent Mannose 6-phosphate receptor in neurodegenerative diseases. Mol Neurobiol 2017;54:2636–58. doi: https://doi.org/10.1007/s12035-016-9849-7.
[48] Nho K, Kueider-Paisley A, Ahmad S, MahmoudianDehkordi S, Arnold M, Risacher SL, et al. Association of altered liver enzymes with alzheimer disease diagnosis, cognition, neuroimaging measures, and cerebrospinal fluid biomarkers. JAMA Netw Open 2019;2:e197978. doi: https://doi.org/10.1001/jamanetworkopen.2019.7978.
[49] Martínez-Reyes I, Chandel NS. Mitochondrial TCA cycle metabolites control physiology and disease. Nat Commun 2020;11:102. doi: https://doi.org/10.1038/s41467-019-13668-3.
[50] Garcia-Fernandez M, Sierra I, Puche JE, Guerra L, Castilla-Cortazar I. Liver mitochondrial dysfunction is reverted by insulin-like growth factor II (IGF-II) in aging rats. J Transl Med 2011;9:123. doi: https://doi.org/10.1186/1479-5876-9-123.
[51] Ahuja M, Kaidery NA, Yang L, Calingasan N, Smirnova N, Gaisin A, et al. Distinct Nrf2 signaling mechanisms of fumaric acid esters and their role in neuroprotection against 1-Methyl-4-Phenyl-1,2,3,6-Tetrahydropyridine-induced experimental parkinson's-like disease. J Neurosci 2016;36:6332–51. doi: https://doi.org/10.1523/JNEUROSCI.0426-16.2016.
[52] Arnold PK, Finley LWS. Regulation and function of the mammalian tricarboxylic acid cycle. J Biol Chem 2023;299:. doi: https://doi.org/10.1016/j.jbc.2022.102838102838.
[53] Dinkova-Kostova AT, Abramov AY. The emerging role of Nrf2 in mitochondrial function. Free Radic Biol Med 2015;88:179–88. doi: https://doi.org/10.1016/j.FREERADBIOMED.2015.04.036.
[54] Esteras N, Dinkova-Kostova AT, Abramov AY. Nrf2 activation in the treatment of neurodegenerative diseases: A focus on its role in mitochondrial bioenergetics and function. Biol Chem 2016;397:383–400. doi: https://doi.org/10.1515/hsz-2015-0295.
[55] Salvi M, Morrice NA, Brunati AM, Toninello A. Identification of the flavoprotein of succinate dehydrogenase and aconitase as in vitro mitochondrial substrates of Fgr tyrosine kinase. FEBS Lett 2007;581:5579–85. doi: https://doi.org/10.1016/j.febslet.2007.11.005.
[56] Van Laar VS, Otero PA, Hastings TG, Berman SB. Potential role of Mic60/Mitofilin in Parkinson's disease. Front Neurosci 2019;12:1–14. doi: https://doi.org/10.3389/fnins.2018.00898.
[57] Tsai PI, Lin CH, Hsieh CH, Papakyrikos AM, Kim MJ, Napolioni V, et al. PINK1 phosphorylates MIC60/Mitofilin to control structural plasticity of mitochondrial crista junctions. Mol Cell 2018;69:744–756.e6. doi: https://doi.org/10.1016/j.molcel.2018.01.026.
[58] Sepúlveda D, Grunenwald F, Vidal A, Troncoso-Escudero P, Cisternas-Olmedo M, Villagra R, et al. Insulin-like growth factor 2 and autophagy gene expression alteration arise as potential biomarkers in Parkinson's disease. Sci Rep 2022;12:2038. doi: https://doi.org/10.1038/s41598-022-05941-1.
[59] Picard M, Shirihai OS. Mitochondrial signal transduction. Cell Metab 2022;34:1620–53. doi: https://doi.org/10.1016/j.cmet.2022.10.008.
[60] John GB, Shang Y, Li L, Renken C, Mannella CA, Selker JML, et al. The mitochondrial inner membrane protein mitofilin controls cristae morphology. Mol Biol Cell 2005;16:1543–54. doi: https://doi.org/10.1091/mbc.e04-08-0697.
[61] Madungwe NB, Feng Y, Lie M, Tombo N, Liu L, Kaya F, et al. Mitochondrial inner membrane protein (mitofilin) knockdown induces cell death by apoptosis via an AIF-PARP-dependent mechanism and cell cycle arrest. Am J Phys Cell Phys 2018;315:C28–43. doi: https://doi.org/10.1152/ajpcell.00230.2017.
[62] Giordano S, Lee J, Darley-Usmar VM, Zhang J. Distinct effects of rotenone, 1-methyl-4-phenylpyridinium and 6-hydroxydopamine on cellular bioenergetics and cell death. PLoS One 2012;7:e44610. doi: https://doi.org/10.1371/journal.pone.0044610.
[63] Risiglione P, Leggio L, Cubisino SAM, Reina S, Paternò G, Marchetti B, et al. High-resolution respirometry reveals mpp+ mitochondrial toxicity mechanism in a cellular model of Parkinson's disease. Int J Mol Sci 2020;21:1–15. doi: https://doi.org/10.3390/ijms21217809.
[64] Imam Aliagan AD, Ahwazi MD, Tombo N, Feng Y, Bopassa JC. Parkin interacts with Mitofilin to increase dopaminergic neuron death in response to Parkinson's disease-related stressors. Am J Transl Res 2020;12:7542–64.
[65] Wang H, Chen Y, Chen J, Zhang Z, Lao W, Li X, et al. Cell cycle regulation of DNA polymerase beta in rotenone-based Parkinson's disease models. PLoS One 2014;9:e109697.
[66] Pizarro JG, Junyent F, Verdaguer E, Jordan J, Beas-Zarate C, Pallàs M, et al. Effects of MPP+ on the molecular pathways involved in cell cycle control in B65 neuroblastoma cells. Pharmacol Res 2010;61:391–9. doi: https://doi.org/10.1016/j.phrs.2010.01.003.
[67] Zhang Z, Cao X, Xiong N, Wang H, Huang J, Sun S, et al. DNA polymerase-β is required for 1-methyl-4-phenylpyridinium-induced apoptotic death in neurons. Apoptosis 2010;15:105–15. doi: https://doi.org/10.1007/s10495-009-0425-8.
[68] Sharma R, Kumar D, Jha NK, Jha SK, Ambasta RK, Kumar P. Re-expression of cell cycle markers in aged neurons and muscles: Whether cells should divide or die? Biochim Biophys Acta (BBA) - Mol Basis Dis 2017;1863:324–36. doi: https://doi.org/10.1016/J.BBADIS.2016.09.010.
[69] Krantic S, Mechawar N, Reix S, Quirion R. Molecular basis of programmed cell death involved in neurodegeneration. Trends Neurosci 2005;28:670–6. doi: https://doi.org/10.1016/j.tins.2005.09.011.
[70] Jackson SP, Bartek J. The DNA-damage response in human biology and disease. Nature 2009;461:1071–8. doi: https://doi.org/10.1038/nature08467.
[71] Zhang Y, Hunter T. Roles of Chk1 in cell biology and cancer therapy. Int J Cancer 2014;134:1013–23. doi: https://doi.org/10.1002/ijc.28226.
[72] Ye W, Blain SW. Chk1 has an essential role in the survival of differentiated cortical neurons in the absence of DNA damage. Apoptosis 2011;16:449–59. doi: https://doi.org/10.1007/s10495-011-0579-z.
[73] Ye W, Blain SW. S phase entry causes homocysteine-induced death while ataxia telangiectasia and Rad3 related protein functions anti-apoptotically to protect neurons. Brain 2010;133:2295–312. doi: https://doi.org/10.1093/brain/awq139.
[74] Oshikawa M, Okada K, Tabata H, Nagata KI, Ajioka I. Dnmt1-dependent Chk1 pathway suppression is protective against neuron division. Development (Cambridge) 2017;144:3303–14. doi: https://doi.org/10.1242/dev.154013.
[75] Hu W, Wang Z, Zhang H, Mahaman YAR, Huang F, Meng D, et al. Chk1 inhibition ameliorates Alzheimer's disease pathogenesis and cognitive dysfunction through CIP2A/PP2A signaling. Neurotherapeutics 2022;19:570–91. doi: https://doi.org/10.1007/s13311-022-01204-z.
[76] Takai H, Tominaga K, Motoyama N, Minamishima YA, Nagahama H, Tsukiyama T, et al. Aberrant cell cycle checkpoint function and early embryonic death in Chk1(-/-) mice. Genes Dev 2000;14:1439–47.
[77] Kinger S, Dubey AR, Kumar P, Jagtap YA, Choudhary A, Kumar A, et al. Molecular chaperones' potential against defective proteostasis of amyotrophic lateral sclerosis. Cells 2023;12. doi: https://doi.org/10.3390/cells12091302.